Microchimica Acta (2021) 188:270
https://doi.org/10.1007/s00604-021-04938-3

ORIGINAL PAPER

Rationally engineered high-performance $BiVO_4/Ag_3VO_4/SnS_2$ photoelectrodes for ultrasensitive immunosensing of CYFRA21-1 based on HRP-tyramine-triggered insoluble precipitates

Dongquan Leng[1] · Rui Xu[1] · Lei Liu[1] · Huan Wang[1] · Jingshuai Li[1] · Xiang Ren[1] · Qin Wei[1] · Huangxian Ju[1,2]

Received: 10 April 2021 / Accepted: 9 July 2021

Abstract

A photoelectrochemical (PEC) biosensor capable of detecting cytokeratin 19 fragment 21-1 (CYFRA21-1) was optimized by taking advantage of the powerful conjugate repeats of horseradish peroxidase and tyramine (HRP-tyramine)–triggered enzymatic biocatalytic precipitation (BCP) on high-performance $BiVO_4/Ag_3VO_4/SnS_2$ photoelectrodes. Compared with the ubiquitous BCP strategy, we identified a design supporting conjugate repeats generated by HRP and tyramine–triggered immeasurable insoluble precipitates in the presence of hydrogen peroxide and 4-chloro-1-phenol (4-CN), and the steric hindrance improved sensitivity. Moreover, by virtue of $BiVO_4$, Ag_3VO_4, SnS_2 excellent level matching structure and chemical stability, a heterojunction ($BiVO_4/Ag_3VO_4/SnS_2$) with high light absorption efficiency has been successfully prepared. The novel heterostructure system of $BiVO_4/Ag_3VO_4/SnS_2$ with high detection current and low background signal exhibited high-performance PEC determination. Generally, the hitherto untapped biosensor resource realized the sensitive detection of CYFRA21-1 with a wide linear range from 50 fg/mL to 200 ng/mL, and a detection limit of 15 fg/mL, which illustrated the potential for biotechnological applications.

Keywords Photoelectrochemistry · Immunoassay · Ag_3VO_4 · HRP-tyramine · Biocatalysis · CYFRA21-1

Introduction

Since the beginning of the new century, cancer has become a disease with high frequency. Due to the asymptomatic characteristic in the early stage, cancer patients cannot get timely and effective treatment. Therefore, it is an urgent task to construct a simple and rapid method to detect disease markers [1, 2]. In recent years, for the detection of disease markers, many promising technologies have been developed in the field of biosensor analysis [3–7]. The constructions of these sensors have achieved the detection of disease markers to a certain extent. However, in order to pursue the advantages of future miniaturization of sensors, low background signal, and rapid detection, a photoelectrochemical (PEC) immunosensor is constructed for non-small cell lung cancer marker (CYFRA21-1) detection in this work. The PEC sensor is a device that outputs light signals as readable electrical signals [8–10]. When the light stimulates to the photoelectric material, the energy of the photons is given to the electrons, which results in the transition of electrons from valence band to conduction band; the photo-generated electrons are generated, and they further produce photocurrent [11–14]. In this detection mode, a series of signal amplification strategies can be carried out on the substrate material through loading specific disease markers. For example, Xu et al. used the specific binding of antigen and antibody on the photoelectric material to hinder the electron exchange between the substrate materials and the electrolyte [15]. Zhao et al. and Yang et al. used

✉ Jingshuai Li
lijings19910719@163.com

✉ Xiang Ren
chem_renx@163.com

✉ Qin Wei
sdjndxwq@163.com

[1] Collaborative Innovation Center for Green Chemical Manufacturing and Accurate Detection; Key Laboratory of Interfacial Reaction & Sensing Analysis in Universities of Shandong, School of Chemistry and Chemical Engineering, University of Jinan, Jinan 250022, People's Republic of China

[2] State Key Laboratory of Analytical Chemistry for Life Science, Department of Chemistry, Nanjing University, Nanjing 210023, People's Republic of China

Published online: 23 July 2021

nano-mimetic enzyme as the marker labeled on secondary antibody; it can absorb light energy competed with substrate materials [8, 16]. However, the nano-mimetic enzyme has slightly inferior catalytic activity as biological enzymes to achieve signal amplification, and the low activity of the mimic enzyme results in low sensitivity. Fortunately, horseradish peroxidase (HRP)–based tyramine amplification has been applied in electrochemical immunoassay [17], electrochemiluminescence immunoassay [18], and chemiluminescence biosensors [19], but the field of PEC sensors has not yet been explored. Therefore, based on the work of the abovementioned research group, we further optimized the detection scheme to realize the sensitive detection of CYFRA21-1.

In this work, SiO_2 nanospheres (SiO_2 NSs) coupled with HRP were co-modified on secondary antibody (Ab_2) to form the bioconjugate HRP-SiO_2-Ab_2. This conjugate could react with the followed HRP-tyramine to trigger HRP conjugate repeats under the excitation of hydrogen peroxide. At the same time, insoluble precipitates (4-CD) under the catalysis of HRP was generated when the electrode was placed in a solution containing 4-chloro-1-phenol (4-CN). The steric hindrance of HRP-SiO_2-Ab_2, enzyme amplification strategy of HRP-tyramine conjugate repeats, and the insoluble precipitates of 4-CD greatly hindered the transmission of electron donors and extremely changed the value of the photocurrent. Thus, the obtained sensor realized the super sensitivity of CYFRA21-1 detection.

The requirements of substrate materials for PEC signal amplification sensors are extremely harsh, and the biocompatibility, photosensitive performance, electron-hole composite, and the stability of the materials must be taken into account [20–22]. $BiVO_4$ [23] has attracted wide attention due to its excellent characteristics, such as narrow band gap, low toxicity, and chemical stability. However, pure $BiVO_4$ with excessive recombination of charge carriers and poor carrier transport performance impedes practical application; thus, it needs a modification of other materials to obtain efficient photoelectric conversion efficiency. The band gap of Ag_3VO_4 matched with the $BiVO_4$ energy level makes it possible to broaden the absorption of visible light [24, 25]. In addition, ternary heterojunction combining SnS_2 with $BiVO_4$/Ag_3VO_4 has a perfect bandgap matching structure, which can further improve the efficiency of electron transmission, and provides infinite possibilities for our innovative signal amplification strategy sensors [26–28]. Therefore, based on HRP-tyramine-triggered enzymatic biocatalytic precipitation (BCP) on high-performance $BiVO_4$/Ag_3VO_4/SnS_2 photoelectrodes, the prepared ultrasensitive photoelectrochemical immunoassay of CYFRA21-1 achieved a wide linear range and low detection limit. The construction process of the immunosensor is showed in Scheme 1.

Experimental section

Materials and apparatus

Reagents and equipment and more experimental information are found in the Supplementary information.

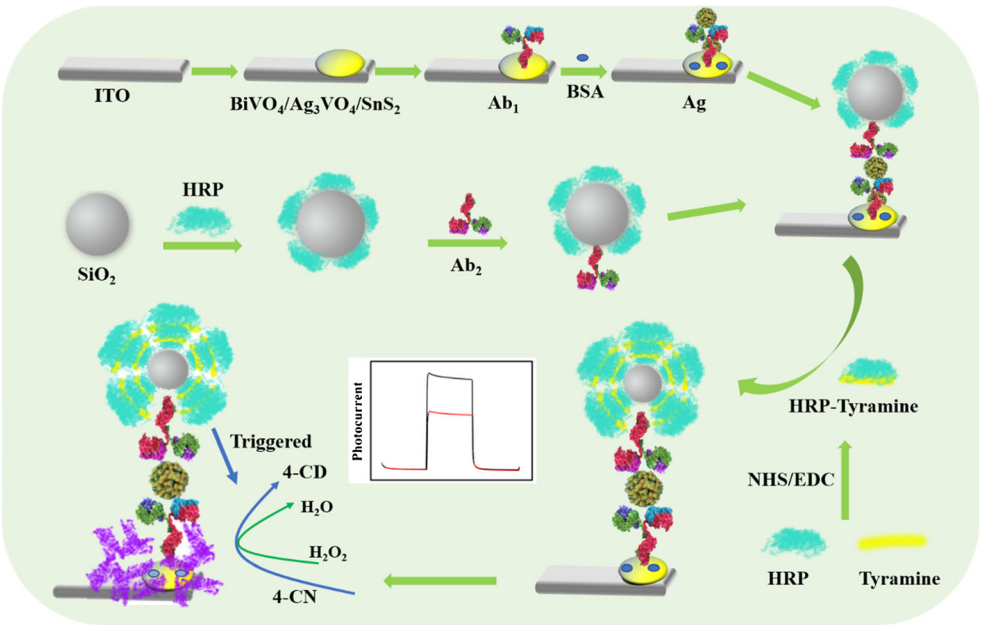

Scheme 1 Fabrication process of photoelectrochemical immunosensor

Preparation of $BiVO_4$ and $BiVO_4/Ag_3VO_4$

The synthesis process was modified based on the reference [29]. Firstly, 0.06 g of bismuth nitrate pentahydrate and 0.046 g of sodium orthovanadate were dissolved in 40 mL of ultrapure water. The mixed solution reacted at 160 °C for 8 h in a Teflon-lined autoclave, after sonication for 20 min. When the reaction cooled to 25 °C, it was washed by using absolute ethanol and ultrapure water for 5 times, and then was vacuum-dried to obtain product powder ($BiVO_4$).

In total, 0.32 g $BiVO_4$ was dissolved in 50 mL of ultrapure water, then 0.12 g of silver nitrate was added with stirring for 30 min. And then, we dissolved 0.044 g of sodium orthovanadate in 50 mL of ultrapure water and stirred for 30 min; then this solution was slowly dropped into the above $BiVO_4$ solution, stirring for 3 h in the dark. After being washed and vacuum-dried for 10 h at 60 °C, $BiVO_4/Ag_3VO_4$ was obtained.

Preparation of HRP-tyramine

A total of 1.2 mL of HRP solution (1 mg/mL) was mixed in 3 mL of *N*-2-hydroxyethylpiperazine-*N*′-2-ethanesulfonate, and was shaken for 5 min; then the pH of 3 M hydrochloric acid solution was adjusted to 7.3. Then 30 mg NHS and 40 mg EDC were added while shaking for 45 min. Subsequently, 1.2 mL of tyramine (5 mg/mL) was added drop by drop into the mixture, and was shaken for 12 h at 25 °C, and then the resulting solution was dialyzed in 0.1 M PBS solution with pH of 7.4 for 24 h. The obtained HRP-tyramine solution was stored at 4 °C. Other details of material preparation processes are shown in the "Supplementary information" file.

Preparation of photoelectrochemical sensor

Firstly, the ITO was ultrasonically cleaned with washing powder, acetone, ultrapure water, and ethanol in sequence, and dried in an oven at 70 °C. Ten microliters of $BiVO_4/Ag_3VO_4$ and SnS_2 (5 mg/mL) was added dropwise to the conductive surface of the ITO in sequence, dried under infrared light, and then burned in the air at 250 °C for 2 h. Then on the surface of electrode, we dropped 10 μL of thioglycolic acid (TGA, 3 mM) and was incubated for 0.5 h, and then added 10 μL of the mixture (15 mg/mL NHS and 30 mg/mL EDC). An hour later, the electrode surface was washed with PBS (pH = 7.4) and dried at room temperature until it became a wet film. Then adding 10 μL, 10 μg/mL of CYFRA21-1 capture antibody (Ab_1) was placed at room temperature for an hour. Ten microliters of the prepared BSA (1%) solution was added to incubate for an hour. Ten microliters of CYFRA21-1 antigen was dropped to incubate for 40 min, and then 10 μL of Ab_2-SiO_2-HRP was added after 40 min. Subsequently, 7 μL of HRP-tyramine and 3 μL of H_2O_2 (4 mM) were added on the electrode for 20 min. Finally, the finished electrode was soaked in the solution with 4-CN (10 mM) and 0.15 mM H_2O_2 for 15 min (Scheme 1).

Photoelectrochemical sensor detection

Electrochemical workstation was used to test with three electrode systems, the prepared ITO modified sensor as a working electrode in PBS buffer solution containing 0.1 M electron donor (ascorbic acid). The i-t method was utilized to detect the CYFRA21-1 antigen standard solution prepared by successive dilutions with PBS, setting the voltage to 0 V, run time 65 s, and the light source which is a white mixed light (400–700 nm). After the electrodes were placed, turning on the light for 10 s and continuing to irradiate for 10 s, recording the photocurrent, and a series of detection tasks were completed continuously.

Results and discussion

Characterization of materials

To prove the photoelectric substrate materials were successfully prepared, here, physical characterizations were performed for all the prepared solutions. The X-ray diffraction (XRD) patterns were carried out to explore the crystallographic structure, and the results are shown in Fig. 1A ($BiVO_4$ and $BiVO_4/Ag_3VO_4$) and Fig. S1A (SnS_2). Pure $BiVO_4$ showed peaks characteristic of monoclinic $BiVO_4$ (PDF No.75-1867); when Ag_3VO_4 was composited with $BiVO_4$, the intensities of the diffraction peaks corresponding to the (121), (−213) and (−512) crystal planes of Ag_3VO_4 emerged [29, 30]. Electron microscopy images were taken for photoelectric nanomaterials with various compositions ($BiVO_4$, $BiVO_4/Ag_3VO_4$, SnS_2) to display their morphological attributes. Specifically, the mean nanorods' length shifted from 200 to 300 nm as deduced from the histograms in Fig. 1B. SEM (Fig. 1C) and TEM (Fig. 1E and F) images confirmed that the Ag_3VO_4 nanocrystallites were evenly dispersed on the $BiVO_4$ nanorods. An SEM image was also taken for the bare SnS_2 (Fig. 1D); in the figure, we can clearly see that SnS_2 presented the nanoflower morphology with the large specific surface. Moreover, the mapping image of $BiVO_4/Ag_3VO_4$ (Fig. S2) revealed the existence of Bi, Ag, V, and O elements. The scans of Bi, Ag, V, and O further proved the Ag_3VO_4 random distribution on $BiVO_4$ surface. XPS was employed to confirm the chemical valence of the $BiVO_4/Ag_3VO_4$. Figure 1G shows that the two strong peaks at 164.1 eV and 158.8 eV are assigned to $4f_{5/2}$ and $4f_{7/2}$ of Bi, respectively. The 3D peaks located at 367.3 and 373.6 eV should originate from Ag_3VO_4 (Fig. 1H), which demonstrated that the silver species is Ag^+ cations. The peaks of 516.7 and 524.1 eV were consistent with V^{5+} in Fig. 1I. The predominant

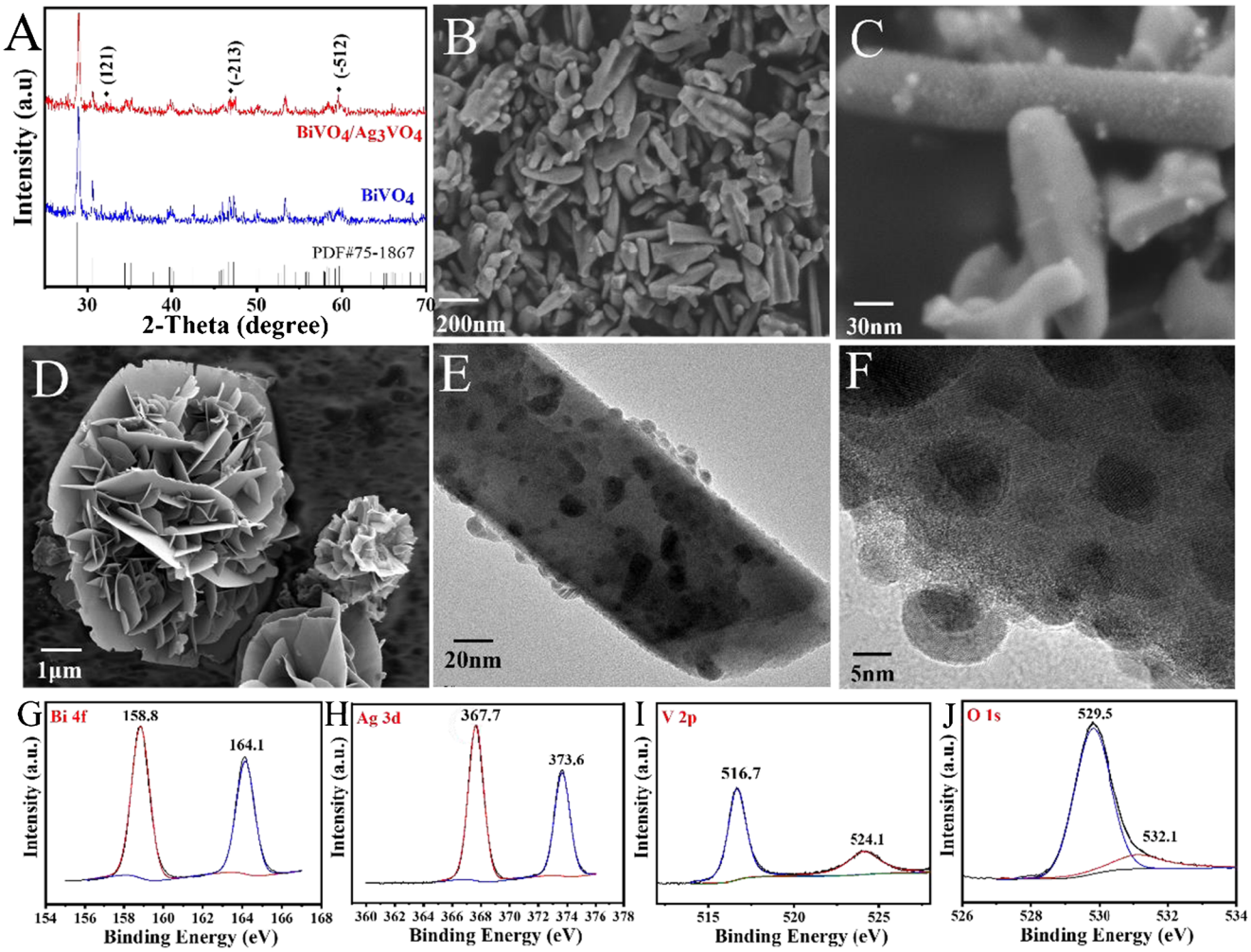

Fig. 1 (**A**) XRD image of $BiVO_4$ and $BiVO_4/Ag_3VO_4$, (**B**) SEM image of $BiVO_4$, (**C**) SEM image of $BiVO_4/Ag_3VO_4$, (**D**) SEM image of SnS_2, (**E**) and (**F**) TEM image of $BiVO_4/Ag_3VO_4$, (**G**) XPS spectra of Bi 4f, (**H**) XPS spectra of Ag 3d, (**I**) XPS spectra of V 2p, and (**J**) XPS spectra of O 1 s

peak (Fig. 1J) of O 1 s (529.5 eV) was attributed to the lattice oxygen, and the other O 1 s peak can be belonged to the O in H_2O (532.1 eV). The survey spectrum of $BiVO_4/Ag_3VO_4$ is shown in Fig. S1B. The constructions of $BiVO_4/Ag_3VO_4$ and SnS_2 were prepared successfully through the confirmation of the above results.

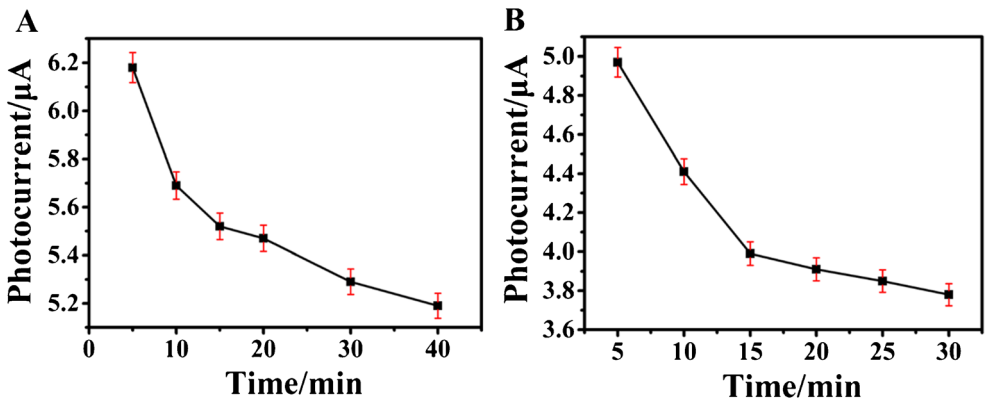

Fig. 2 **A** The time of HRP-tyramine conjugate repeats generating. **B** The time of soaked in 4-CN solution. $c_{CYFRA21\text{-}1}$ = 10 ng/mL, error bars = SD ($n = 3$)

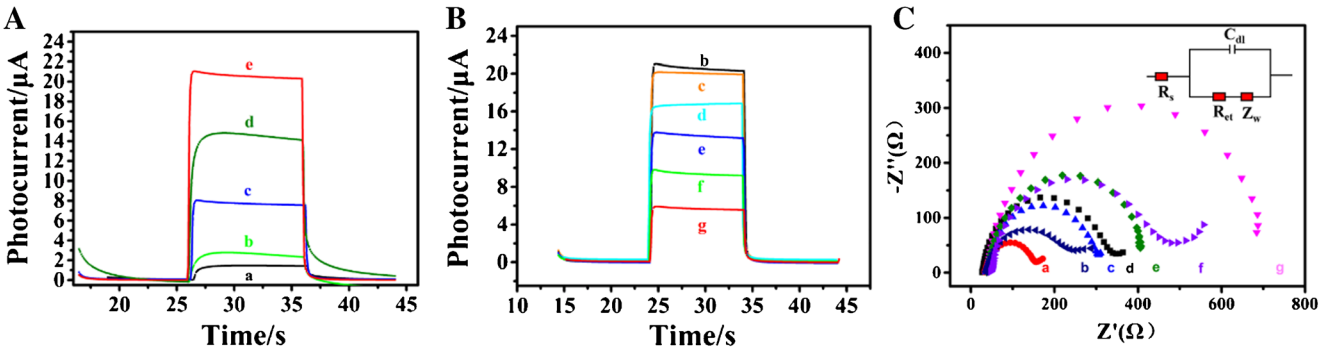

Fig. 3 (**A**) PEC signal of (a) ITO/$BiVO_4$, (b) ITO/$BiVO_4$/Ag_3VO_4, (c) ITO/SnS_2, (d) ITO/$BiVO_4$/SnS_2, (e) ITO/$BiVO_4$/Ag_3VO_4/SnS_2. (**B**) The change of PEC signal and (**C**) Nyquist diagrams of (a) ITO/$BiVO_4$/Ag_3VO_4 (b) ITO/$BiVO_4$/Ag_3VO_4/SnS_2, (c) ITO/$BiVO_4$/Ag_3VO_4/SnS_2/Ab_1, (d) ITO/$BiVO_4$/Ag_3VO_4/SnS_2/Ab_1/Ag, (e) ITO/$BiVO_4$/Ag_3VO_4/SnS_2/Ab_1/Ag/HRP-SiO_2-Ab_2, (f) ITO/$BiVO_4$/Ag_3VO_4/SnS_2/Ab_1/Ag/HRP-SiO_2-Ab_2/HRP-tyramine, (g) ITO/$BiVO_4$/Ag_3VO_4/SnS_2/Ab_1/Ag/HRP-SiO_2-Ab_2/HRP-tyramine/4-CD ($c_{CYFRA21\text{-}1}$ = 0.001 ng/mL). Inset in C:equivalent circuit for EIS.

Optimization of the experimental conditions

The stage of HRP-tyramine conjugate repeats involves the complex process of tyramine generating radical intermediates under the excitation of H_2O_2, and then HRP-tyramine conjugate repeats generated on SiO_2 NSs; therefore, the incubation time is important. Here, we used the concentration 10 ng/mL of Ag and 4 mM of H_2O_2 for the test. Five, 10, 15, 20, 30 and 40 min were selected for optimization. Figure 2A proves that the photocurrent dropped rapidly in the first 10 min, and then it showed a relatively slow decline; in the case of comprehensive consideration, we finally selected 20 min as the incubation time to generate conjugate repetition.

The conjugate repeats generated on SiO_2 NSs and the excitation of H_2O_2 will convert 4-CN into insoluble 4-CD precipitation, and the precipitation conversion time was selected. Five, 15, 20, 25 and 30 min were selected as the time optimization. In Fig. 2B, it can be clearly understood that the precipitate generation occurred in the first 15 min under the catalysis of HRP, while the subsequent time process was extremely slow (c = 10 ng/mL). Therefore, 15 min was selected as the time point for the precipitate generation.

Characterization of the immunosensor

In this work, each modification was characterized by photocurrent and impedance to represent the successful construction of the sensor. In Fig. 3A, we could get clear information that the construction of the $BiVO_4$/Ag_3VO_4/SnS_2 heterojunction greatly improved the photoelectric efficiency compared with each individual material (a: ITO/$BiVO_4$, b: ITO/$BiVO_4$/Ag_3VO_4, c: ITO/SnS_2, d: ITO/$BiVO_4$/SnS_2, e: ITO/$BiVO_4$/Ag_3VO_4/SnS_2). Photocurrent (Fig. 3B) and impedance (Fig. 3C) tests were performed to confirm the sensor construction process (ITO/$BiVO_4$/Ag_3VO_4, ITO/$BiVO_4$/Ag_3VO_4/SnS_2, Ab_1, Ag, HRP-SiO_2-Ab_2, HRP-tyramine and 4-CD were further appended to the previous step from a to g). In Fig. 3C from a to g, the modification sequence in impedance test was

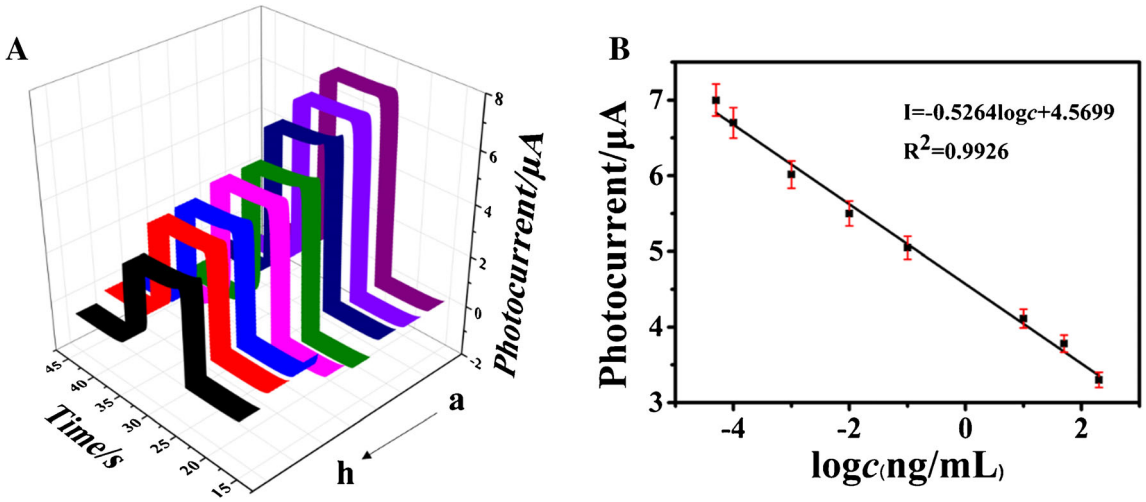

Fig. 4 (**A**) PEC response and (**B**) calibration plot of ITO/$BiVO_4$/Ag_3VO_4/SnS_2 electrode toward CYFRA21-1 at different concentrations. (a–f) 0.00005, 0.0001, 0.001, 0.01, 0.1, 10, 50, and 200 ng/mL. Error bars = SD (n = 3)

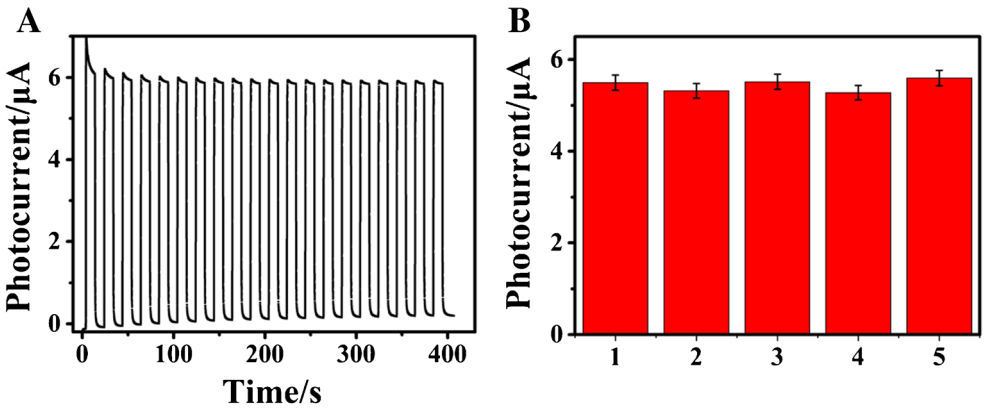

Fig. 5 **A** Stability test of the sensor ($c_{CYFRA21\text{-}1}$ = 0.001 ng/mL). **B** The reproducibility ($c_{CYFRA21\text{-}1}$ = 0.01 ng/L). Error bars = SD (n = 3)

consistent with Fig. 3B; it could be seen that each step of the modification of the sensor was successful.

CYFRA21-1 analysis

After exploring the electron transfer mechanism of the biosensor, the strategy was used for signal detection for CYFRA21-1 under the experimental conditions described above (Fig. 4A). In a nutshell, the concentration of the antigen was expressed in the form of photocurrent. Data analysis based on the relationship between antigen concentration and obtained photocurrent was utilized, and the equation was $I = 4.5699–0.5264 \log c$ (ng/mL, linear range from 50 fg/mL to 200 ng/mL), and the correlation coefficient was 0.9926. According to the method of signal-to-noise ratio of 3 ($S/N = 3$), the limit of detection (LOD) could be calculated, and 15 fg/mL was confirmed (Fig. 4B). For the detection range and detection limit of this signal amplification strategy, we have made a detailed comparison (Table S1) between this and the other sensors with excellent performance. From Table S1, we can clearly understand that the sensor has obviously competitive advantages in marker detection. Moreover, in order to further demonstrate the advantages of the high-performance materials, the materials used in this work were compared with other sensors, and the result (Table S2) showed that the sensor based on $BiVO_4/Ag_3VO_4/SnS_2$ has obvious advantages.

Reproducibility and stability

Repeatability and stability are another extremely important characteristic factors for the application of biosensors in clinical diagnosis. The sensors prepared here were tested continuously 20 times with turning the excitation light on and off ($c_{CYFRA21–1}$ = 0.001 ng/mL). Figure 5A clearly shows that the sensor was extremely stable. The repeatability experiment was performed 5 times at the Ag concentration of 0.01 ng/mL, and 2.26% of the relative standard deviation (RSD) was obtained, which obviously indicates the reproducibility of the immunosensor. The photocurrent of proposed sensor (Fig. S4 A) maintained 98.8%, 97.9%, 96.7%, 95.6%, and 93.8% of its initial photocurrent after storing at 4 °C for 3 days, 6 days, 9 days, 12 days, and 15 days, respectively, proving good long-time stability. In addition, the operating lifetime was tested under the visible light irradiation of 400 s, which proved that there was no significant photocurrent attenuation in Fig. S4 B.

Real sample analysis

Clinical application is the ultimate goal of all the work done above; therefore, real sample detection was carried out. CYFRA21-1 of different concentrations (0.01, 0.05, 1.0, 10, 100 ng/mL) in human serum was tested, and the results are shown in Table S3. The range of 2.84–4.90% of RSD can be obtained from Table S2, and the recovery rate can be achieved 96.6–103.4%. According to the result obtained, clinical diagnostic potential has been demonstrated in real serum samples, but the performance of sensors may need to be further enhanced in the face of more complex serum samples.

Conclusion

In this work, a new signal amplification photoelectrochemical immunoassay based on HRP-tyramine conjugate repeats–triggered enzymatic biocatalytic precipitation on SiO_2 NSs was designed for ultrasensitive detection of a tumor marker (CYFRA21-1) with high-performance $BiVO_4/Ag_3VO_4/SnS_2$ as the substrate material. The HRP-SiO_2-Ab_2, HRP-tyramine conjugate repeats, and 4-CD greatly hindered the transmission of electron donors and extremely sensitively changed the photocurrent. Therefore, the work realized the sensitive detection of CYFRA21-1 with a wide linear range from 50 fg/mL to 200 ng/mL, and the detection limit of 15 fg/mL. In the future, we will apply this immunosensor to more and more complex human serum samples in order to further enhance the ability of the sensor for clinical application. This informative idea of using HRP-tyramine conjugate to increase the amount of

substrate catalyzed per unit modified area may inspire more possibilities for improvement of sensitivity in biosensing and immunoassays..

Supplementary Information The online version contains supplementary material available at https://doi.org/10.1007/s00604-021-04938-3.

Acknowledgements We appreciate the support of the National Key Scientific Instrument and Equipment Development Project of China (No. 21627809), National Natural Science Foundation of China (No. 21777056), Special Foundation for Taishan Scholar Professorship of Shandong Province, Jinan Scientific Research Leader Workshop Project (2018GXRC024), Innovation Team Project of Colleges and Universities in Jinan (No.2019GXRC027).

Declarations

Conflict of interest The authors have no relevant financial or non-financial interests to disclose.

References

1. Su J, Wu F, Xia H, Wu Y, Liu S (2020) Accurate cancer cell identification and microrna silencing induced therapy using tailored DNA tetrahedron nanostructures. Chem Sci 11:80–86
2. Zhou S, Hu T, Han G, Wu Y, Hua X, Su J et al (2020) Accurate cancer diagnosis and stage monitoring enabled by comprehensive profiling of different types of exosomal biomarkers: surface proteins and mirnas. Small 16:e2004492
3. Zhan Y, Yang S, Luo F, Guo L, Zeng Y, Qiu B, Lin Z (2020) Emission wavelength switchable carbon dots combined with biomimetic inorganic nanozymes for a two-photon fluorescence immunoassay. ACS Appl Mater Interfaces 12:30085–30094
4. Yang L, Fan D, Zhang Y, Ding C, Wu D, Wei Q, Ju H (2019) Ferritin-based electrochemiluminescence nanosurface energy transfer system for procalcitonin detection using hwrgwvc heptapeptide for site-oriented antibody immobilization. Anal Chem 91:7145–7152
5. Xu R, Du Y, Leng D, Liu L, Li Y, Ren X et al (2020) Antigen down format photoelectrochemical analysis supported by fullerene functionalized Sn_3O_4. Chem Commun 56:7455–7458
6. Qian Y, Feng J, Xu R, Fan D, Du Y, Ren X et al (2020) Zinc and molybdenum co-doped bivo4 nanoarray for photoelectrochemical diethylstilbestrol analysis based on the dual-competitive system of manganese hexacyanoferrate hydrate nanocubes. ACS Appl Mater Interfaces 12:16662–16669
7. Feng J, Qian Y, Cheng Q, Ma Y, Wu D, Ma H, Ren X, Wang X, Wei Q (2020) A signal amplification of p DNA@Ag_2S based photoelectrochemical competitive sensor for the sensitive detection of OTA in microfluidic devices. Biosens Bioelectron 168:112503
8. Yang R, Zou K, Li Y, Meng L, Zhang X, Chen J (2018) Co_3O_4-Au polyhedra: a multifunctional signal amplifier for sensitive photoelectrochemical assay. Anal Chem 90:9480–9486
9. Zhao C-Q, Ding S-N (2019) Perspective on signal amplification strategies and sensing protocols in photoelectrochemical immunoassay. Coord Chem Rev 391:1–14
10. Leng D, Li J, Xu R, Liu L, Liu X, Fan D, Wang H, Wei Q, Ju H (2020) THCH as electron donor in controlled-release system for procalcitonin analysis based on $Bi_2Sn_2O_7$ photoanode. Sensors Actuators B Chem 321:128509
11. Shu J, Tang D (2020) Recent advances in photoelectrochemical sensing: from engineered photoactive materials to sensing devices and detection modes. Anal Chem 92:363–377
12. Tan J, Peng B, Tang L, Zeng G, Lu Y, Wang J, Ouyang X, Zhu X, Chen Y, Feng H (2020) CuS QdS/Co_3O_4 polyhedra-driven multiple signal amplifications activated h-BN photoeletrochemical biosensing platform. Anal Chem 92:13073–13083
13. Xu R, Liu L, Liu X, Li Y, Feng R, Wang H, Fan D, Wu D, Wei Q (2020) Novel electron donor encapsulation assay based on the split-type photoelectrochemical interface. ACS Appl Mater Interfaces 12:7366–7371
14. Xu H, Shang H, Liu Q, Wang C, Di J, Chen C et al (2021) Dual mode electrochemical-photoelectrochemical sensing platform for hydrogen sulfide detection based on the inhibition effect of titanium dioxide/bismuth tungstate/silver heterojunction. J Colloid Interface Sci 581:323–333
15. Xu R, Feng R, Wei D, Yan T, Zhang Y, Cao W, Fan D, Wei Q, Ju H (2019) A novel photoelectrochemical singal amplification assay for procalcitonin detection based on $Zn_xBi_2S_{3+x}$ sensitized $NiTiO_3$ matrix. Sensors Actuators B Chem 301:127099
16. Zhao J, Fu C, Huang C, Zhang S, Wang F, Zhang Y, Zhang L, Ge S, Yu J (2021) Co_3O_4-Au polyhedron mimic peroxidase- and cascade enzyme-assisted cycling process-based photoelectrochemical biosensor for monitoring of mirna-141. Chem Eng J 406:126892
17. Zhou J, Tang J, Chen G, Tang D (2014) Layer-by-layer multienzyme assembly for highly sensitive electrochemical immunoassay based on tyramine signal amplification strategy. Biosens Bioelectron 54:323–328
18. Chen F, Wang D, Chen J, Ling J, Yue H, Gou L, Tang H (2020) Ptni nanocubes-catalyzed tyramine signal amplification electrochemiluminescence sensor for nonenzymatic and ultrasensitive detection of hepatocellular carcinoma cells. Sensors Actuators B Chem 305:127472
19. Zhao LZ, Fu YZ, Ren SW, Cao JT, Liu YM (2020) A novel chemiluminescence imaging immunosensor for prostate specific antigen detection based on a multiple signal amplification strategy. Biosens Bioelectron 171:112729
20. Zhang B, Wang H, Xi J, Zhao F, Zeng B (2020) Novel $Bi_{2+x}WO_6$ p-n homojunction nanostructure: preparation, characterization, and application for a self-powered cathodic photoelectrochemical immunosensor. ACS Sens 5:2876–2884
21. Zhang L, Shi XM, Xu YT, Fan GC, Liang YY, Wang C, Zhao WW (2019) Gold nanoparticle-induced photocurrent quenching and recovery of polymer dots: toward signal-on energy-transfer-based photocathodic bioanalysis of telomerase activity in cell extracts. Anal Chem 91:6403–6407
22. Long D, Li M, Wang H, Wang H, Chai Y, Li Z, Yuan R (2020) Ultrasensitive photoelectrochemical assay for DNA detection based on a novel SnS_2/Co_3O_4 sensitized structure. Anal Chem 92:14769–14774
23. Xu Y, Wen Z, Wang T, Zhang M, Ding C, Guo Y, Jiang D, Wang K (2020) Ternary z-scheme heterojunction of Bi SPR-promoted $BiVO_4$/g-C_3N_4 with effectively boosted photoelectrochemical activity for constructing oxytetracycline aptasensor. Biosens Bioelectron 166:112453
24. Gao M, Sun L, Ma C, Li X, Jiang H, Shen D, Wang H, Huo P (2021) Constructed z-scheme g-C_3N_4/Ag_3VO_4/RGO photocatalysts with multi-interfacial electron-transfer paths for high photoreduction of CO_2. Inorg Chem 60:1755–1766
25. Zhang S, Zheng H, Sun Y, Li F, Li T, Liu X, Zhou Y, Chen W, Ju H (2020) Oxygen vacancies enhanced photoelectrochemical aptasensing of 2, 3′, 5, 5′-tetrachlorobiphenyl amplified with Ag_3VO_4 nanoparticle-TiO_2 nanotube array heterostructure. Biosens Bioelectron 167:112477
26. Zhang G, Shan D, Dong H, Cosnier S, Al-Ghanim KA, Ahmad Z et al (2018) DNA-mediated nanoscale metal-organic frameworks

for ultrasensitive photoelectrochemical enzyme-free immunoassay. Anal Chem 90:12284–12291
27. Wu Y, Su H, Yang J, Wang Z, Li D, Sun H, Guo X, Yin S (2020) Photoelectrochemical immunosensor for sensitive detection of alpha-fetoprotein based on a graphene honeycomb film. J Colloid Interface Sci 580:583–591
28. Wei J, Chang W, Qileng A, Liu W, Zhang Y, Rong S, Lei H, Liu Y (2018) Dual-modal split-type immunosensor for sensitive detection of microcystin-LR: enzyme-induced photoelectrochemistry and colorimetry. Anal Chem 90:9606–9613
29. Zhao W, Feng Y, Huang H, Zhou P, Li J, Zhang L, Dai B, Xu J, Zhu F, Sheng N, Leung DYC (2019) A novel z-scheme Ag_3VO_4/$BiVO_4$ heterojunction photocatalyst: study on the excellent photocatalytic performance and photocatalytic mechanism. Appl Catal B Environ 245:448–458
30. Wang Q, Zhou M, Zhang L (2020) A dual mode photoelectrochemical sensor for nitrobenzene and l-cysteine based on 3D flower-like Cu_2SnS_3@SnS_2 double interfacial heterojunction photoelectrode. J Hazard Mater 382:121026